MANCHESTER 1824
The University of Manchester

The University of Manchester Research

Caloric restriction modifies spatiotemporal calcium dynamics in mouse hippocampal astrocytes

DOI:
10.1016/j.bbamcr.2021.119034

Document Version
Accepted author manuscript

Link to publication record in Manchester Research Explorer

Citation for published version (APA):
Denisov, P., Popov, A., Brazhe, A., Lazareva, N., Verkhratsky, A., & Semyanov, A. (2021). Caloric restriction modifies spatiotemporal calcium dynamics in mouse hippocampal astrocytes. *Biochimica et Biophysica Acta - Molecular Cell Research*, *1868*(7), 119034. https://doi.org/10.1016/j.bbamcr.2021.119034

Published in:
Biochimica et Biophysica Acta - Molecular Cell Research

Citing this paper
Please note that where the full-text provided on Manchester Research Explorer is the Author Accepted Manuscript or Proof version this may differ from the final Published version. If citing, it is advised that you check and use the publisher's definitive version.

General rights
Copyright and moral rights for the publications made accessible in the Research Explorer are retained by the authors and/or other copyright owners and it is a condition of accessing publications that users recognise and abide by the legal requirements associated with these rights.

Takedown policy
If you believe that this document breaches copyright please refer to the University of Manchester's Takedown Procedures [http://man.ac.uk/04Y6Bo] or contact uml.scholarlycommunications@manchester.ac.uk providing relevant details, so we can investigate your claim.

OPEN ACCESS

Download date:09. Jun. 2022

REVISED Manuscript (text UNmarked)

Click here to view linked References

Caloric restriction modifies spatiotemporal calcium dynamics in hippocampal mouse astrocytes

Pavel Denisov[1,2], Alexander Popov[1,2], Alexey Brazhe[1,3], Natalia Lazareva[4], Alexei Verkhratsky[4,5,6*], Alexey Semyanov[1,3,4*]

[1]Shemyakin-Ovchinnikov Institute of Bioorganic Chemistry, Russian Academy of Sciences, Miklukho-Maklaya street 16/10, Moscow, 117997, Russia;

[2]Faculty of Biology, Nizhny Novgorod University, Nizhny Novgorod, Russia;

[3]Faculty of Biology, Moscow State University, Moscow, Russia;

[4]Sechenov First Moscow State Medical University, Moscow, Russia;

[5]Faculty of Biology, Medicine and Health, The University of Manchester, Manchester, M13 9PT, UK;

[6]Achucarro Center for Neuroscience, IKERBASQUE, Basque Foundation for Science, 48011 Bilbao, Spain & Department of Neurosciences, University of the Basque Country UPV/EHU and CIBERNED, Leioa, Spain;

[*]Send all correspondence to:
Alexej.Verkhratsky@manchester.ac.uk or semyanov@ibch.ru

Abstract

We analyzed spatiotemporal properties of Ca^{2+} signals in protoplasmic astrocytes in the CA1 *stratum radiatum* of hippocampal slices from young (2 - 3 months old) mice housed in control conditions or exposed to a caloric restriction (CR) diet for one month. The astrocytic Ca^{2+} events became shorter in duration and smaller in size; they also demonstrated reduced velocity of expansion and shrinkage following CR. At the same time, Ca^{2+} signals in the astrocytes from the CR animals demonstrated higher amplitude and the faster rise and decay rates. These changes can be attributed to CR-induced morphological remodelling and uncoupling of astrocytes described in our previous study. CR-induced changes in the parameters of Ca^{2+} activity were partially reversed by inhibition of gap junctions/hemichannels with carbenoxolone (CBX). The effect of CBX on Ca^{2+} activity in CR-animals was unexpected because the diet already decreases gap junctional coupling in astrocytic syncytia. It may reflect the blockade of hemichannels also sensitive to this drug. Thus, CR-induced morphological remodelling of astrocytes is at least partly responsible for changes in the pattern of Ca^{2+} activity in the astrocytic network. How such changes in spatiotemporal Ca^{2+} landscape can translate into astrocytic physiology and neurone-glia interactions remains a matter for future studies.

Keywords: astrocyte, caloric restriction, calcium signalling, gap-junctions

Introduction

Astrocytes, the homeostatic cells of the brain and the spinal cord, exhibit a specific type of excitability mediated by intracellular changes in ion concentrations and second messengers, generally known as intracellular excitability [1]. Specific pathways underlying this type of excitability are mainly represented by ionic signalling, mediated by fluctuations in the intracellular concentration of Ca^{2+} ($[Ca^{2+}]_i$), Na^+ and possibly of other ions. Astrocytic Ca^{2+} signalling in the form of $[Ca^{2+}]_i$ transients and propagating Ca^{2+} waves has been discovered *in vitro* in astrocyte cell cultures [2-4]; subsequent experiments characterised underlying molecular pathways operating in brain slices [5, 6] and *in vivo* in the anaesthetised or awake brains [7, 8]. Astrocyte Ca^{2+} signalling is generated by several pathways differentially expressed in different cellular compartments. In the cell soma and primary processes (known as branches), Ca^{2+} signal is primarily generated by Ca^{2+} release from the endoplasmic reticulum mediated by $InsP_3$ receptors [5, 9] and mitochondria through the transient opening of the mitochondrial permeability transition pore [10]. Emptying of the Ca^{2+} stores triggers secondary store-operated Ca^{2+} entry through the stromal interaction molecule (STIM)-Orai complexes [11, 12] or transient receptor potential canonical (TRPC) channels [13]. In contrast, Ca^{2+} signal generation in the distal leaflets depends on Ca^{2+} entry across plasmalemma [14], which is mediated by reversed Na^+/Ca^{2+} exchanger, ionotropic receptors and transient receptor potential ankyrin 1 (TRPA1) channels [9, 15-17]. Another factor affecting evolution and kinetics of astrocytic Ca^{2+} signals is linked to connexon-formed gap junctions [18].

Astrocytes demonstrate a high degree of morphological and functional plasticity, contributing thus to the life-long adaptive remodelling of the central nervous system (CNS). In particular, astrocytes are involved in adult synaptogenesis and synaptic modulation through the release of a variety of molecular factors [19]. Astrocytes also show a high degree of fast morphological remodelling that defines neurotransmitters availability and neurotransmitter spillover, which both are involved in synaptic plasticity [20, 21]. At the same time, astrocytes undergo long-term changes, which affect their morphology and their relations with neighbouring neurones, with synapses and with the neurovascular unit at large. The long-term adaptive changes in astrocytes occur during development and ageing [22]. In particular, the transition from young to adulthood is associated with a substantial increase in astrocytic morphological profiles and in the volume of astrocytic leaflet distal processes that mainly provide for synaptic coverage and hence for synaptic support. Ageing, to the contrary, is associated with the shrinkage of astrocytes and a decrease in peripheral processes and hence in a decrease of synaptic support; these age-dependent changes translate into deficiencies in long-term potentiation (LTP), learning and memory [22, 23]. Another factor affecting brain structure and function is represented by lifestyle, including sensory and physical stimulation and dieting. Exposure of animals to an enriched environment increases astrocyte complexity and improves cognition, increase in astrocytic homeostatic support being arguably one of the underlying mechanisms [24, 25]. Our recent experiments have demonstrated the modifying effect of caloric restrictive diet on hippocampal astrocytes. Exposure of young animals to caloric restriction (CR) for a period of one month led to a significant change in astrocytic morphology manifested in an increase of the volume of distal leaflets of

hippocampal protoplasmic astrocytes. This led to an increase in astrocytic K^+ buffering and glutamate clearance, both contributing to a positive modulation of LTP in CR animals [26]. In addition, CR led to a decrease in expression of major astrocytic connexin Cx43 and in a consequent decrease in gap junctional coupling in hippocampal astrocyte syncytium [26].

Our previous experiments established a link between astrocytic morphology and spatiotemporal properties of $[Ca^{2+}]_i$ dynamics [27]; similarly, changes in gap junctional coupling may influence $[Ca^{2+}]_i$ profiles [5]. Hence in this paper, we investigated the effects of CR on parameters of $[Ca^{2+}]_i$ dynamics in hippocampal astrocytes. To distinguish between the effects of morphological remodelling and astrocyte uncoupling in the syncytium, we have also tested the effect of pharmacological inhibition of connexons.

Materials and methods

Animals

The experiments were performed in two groups of male mice C57BL/6 from the age of 2-3 months. Experiments were approved by the Institute of Bioorganic Chemistry committee for the maintenance and use of laboratory animals. The animals of both groups were held in individual cages for 1 month. Mice of the first groups received food *ad libitum* (control). For each animal, the nutrition was analyzed for a week, and the daily rate was calculated. The amount of food was weighed, and each animal in the second group (CR) was fed 70% of the average daily intake per animal. For all mice in their home cages lights were maintained on a 12 h light/dark cycle.

Before sacrifice, the mice were anaesthetised with isoflurane. The brain was exposed and placed in an ice-cold solution containing (in mM 50 sucrose; 87 NaCl; 2.5 KCl; 8.48 $MgSO_4$; 1.24 NaH_2PO_4; 26.2 $NaHCO_3$; 0.5 $CaCl_2$; 22 D-glucose. The hippocampi were isolated and cut using a vibrating microtome (Microm HM650 V; Thermo Fisher Scientific) into 350 μm thick slices. The slices were left for 1 hour at 34 ° in a solution containing (in mM): 119 NaCl, 2.5 KCl, 1.3 $MgSO_4$, 1 NaH_2PO4, 26.2 $NaHCO_3$, 1 $CaCl_2$, 1.6 $MgCl_2$, 22 mM D-glucose. Experiments were carried out at 34° C in immersion chamber with continuous perfusion (1-3 ml/min) with artificial cerebrospinal fluid (ACSF) containing (in mM): 119 NaCl; 2.5 KCl; 1.3 $MgSO_4$; 1 NaH_2PO_4; 26.2 $NaHCO_3$; 2 $CaCl_2$; 11 D-glucose. All solutions had osmolarity adjusted to 295 ± 5 mOsm and a pH of 7.4. The solution was continuously gassed with a 95% O_2 and 5% CO_2 mixture.

Ca^{2+} imaging

Astrocytic Ca^{2+} activity was recorded with a confocal microscope, Zeiss LSM DuoScan 510, in CA1 *str.radiatum* of acute hippocampal slices pre-incubated with membrane-permeable Ca^{2+} dye, Oregon Green 488 BAPTA-1 AM (OGB, Invitrogen, USA) and an astrocyte-specific marker, sulforhodamine 101 (100 nM, Invitrogen, USA). After preparation, the slices were transferred to a 3 ml incubation chamber with ACSF containing both dyes. OGB was initially dissolved to 0.795 mM in 0.8% Pluronic F-127

in DMSO. Then 3 µl of the dye was added to the chamber. After incubation for 40 - 45 min at 37 °C in the dark, the slices were transferred into the recording/imaging chamber for time-lapse imaging (one frame/s). OGB was excited with a 488 nm argon laser; the fluorescence was detected through a 500 - 530 nm band-pass filter. Sulforhodamine 101 was excited with a 543 nm HeNe laser; the fluorescence was detected through a 650 - 710 nm band-pass filter. The imaging was performed for 10 min at 34 °C in normal ASCF, then 30 dark noise images were recorded. The recording field was 420x420 µm in 512x512 pixels. After recording the spontaneous Ca^{2+} activity, 100 µM carbenoxolone (CBX, Sigma, USA) was added to the ACSF. After 20 min of incubation with CBX, spontaneous Ca^{2+} activity was rerecorded in the same recording field. Recording parameters were kept unchanged for the entire experiment.

Image processing

All image analysis was performed using custom-written Python software. The raw imaging data were first transformed to a standardised form matching Poisson-like pixel intensity statistics. To this end, a linear regression between average value and variance for randomly chosen blocks of pixels in the background provided estimates for constant dark offset (intercept of the x-axis) and gain (slope of the line). After "Poissonisation", imaging data were denoised using a block-based approach developed in the lab. The Anscombe transformation was first applied to the intensity values to mitigate the heteroscedasticity of the raw data. Next, a local denoising step based on truncated singular value decomposition (SVD) transformation was applied to overlapping blocks of pixels. Intensity estimates in the overlapping regions were averaged. This was followed by inverse Anscombe transformation [28] to obtain final intensity estimates.

Slow-changing baseline fluorescence level was calculated by iteratively smoothing fluorescence signal with an L1-spline [29] and at each iteration substituting values f_i deviating for more that than 3 standard deviations from the smoothing curve fs_i with the smoothed values fs_i. This operation was done in each pixel and the resulting fluorescence baseline $F_0(t)$ was used to calculate relative fluorescence changes $(F(t)-F_0(t))/F_0(t)$ denoted as $\Delta F/F$ below. $\Delta F/F$ changes were then thresholded at 3 standard deviations of background fluorescence fluctuations (in the denoised data), and contiguous sets of supra-threshold pixels in time and space were further termed as Ca^{2+} events.

Spatiotemporal characteristics of Ca^{2+} dynamics

Ca^{2+} events were characterised by the following parameters:
1. Ca^{2+} event frequency – total number of events detected during the recording divided by the recording time and normalised to the recorded area (frequency density).
2. Ca^{2+} event duration – number of frames from initiation to the end of an event multiplied by the inter-frame interval.
3. Ca^{2+} event size – entire territory occupied by the event defined as the number of non-zero pixels in maximal intensity projection along the time axis multiplied by the pixel area.

4. Mean expansion/shrinkage rate of Ca^{2+} event. The instantaneous event area was calculated for each frame. The resulting vector of event areas was rescaled by squared spatial resolution and filtered by the first derivative of Gaussian kernel ($\sigma=1.5$ s) to obtain the numerical derivative of the event area over time (*dS/dt*). The average of all positive *dS/dt* values was used as the mean event expansion rate, while the average of all negative *dS/dt* values was used as the mean event shrinkage rate.
5. Peak amplitude of Ca^{2+} signal ($\Delta F/F$) – the highest $\Delta F/F$ value reached within the event.
6. The maximal rise and decay rates of the Ca^{2+} signal. Rise and decay rates were obtained in each pixel as the first derivative of the timecourse of Ca^{2+} signal in this pixel (*d(ΔF/F)/dt*), calculated by convolution of the $\Delta F/F$ signal with the first derivative of the Gaussian kernel (σ=1.5s) along time domain. Positive values were considered as the rise rates, negative – the decay rates. We refer to the absolute maximum (cf. minimum) values of *d(ΔF/F)/dt* overall spatiotemporal voxels belonging to the event as maximum rates of fluorescence rise (cf. fluorescence decay).

Statistics

Statistical analysis was performed with Origin 8 (OriginLab Corp.). Event frequency density data are presented as the mean ± SEM (Fig. 1c), all other data presented as quartiles (box) ± 10th and 90th percentiles (whiskers). The differences between groups were tested with two-way repeated-measures ANOVA (Fig. 1c) and Mann-Whitney test (all other data); $p < 0.05$ was considered significant. N-numbers correspond to the number of animals in each set of experiments. To reduce the number of animals, hippocampal slices obtained from one animal were used in different sets of experiments of this project and different projects carried in the lab. However, only one slice was used for a particular set. n-numbers represent number of individual events pulled from all slices which were used for the plot.

Results

As alluded to before, treatments of young animals with CR initiates the growth of astrocytic processes associated with uncoupling of inter-astrocytic gap-junctions [26]. Our previous experiments have also demonstrated that astrocytic morphology and gap junction coupling strongly influence Ca^{2+} dynamics in the astrocytic network [5, 27]. Hence astrocytic morphological remodelling and uncoupling can affect Ca^{2+} signalling in these cells. To test this possibility, we performed time-lapse two-photon imaging in hippocampal slices stained with Ca^{2+} sensor (OGB, see method section) in two groups of mice: control and CR. Astrocytic Ca^{2+} events were detected in the CA1 *stratum radiatum,* as described previously [23]. Although OGB predominantly labels astrocytes and the majority of Ca^{2+} events which we recorded were astrocytic, we could not entirely exclude a contribution of neuronal Ca^{2+} activity. To circumvent neuronal contribution and to avoid sampling fast neuronal Ca^{2+} transients, we considered only Ca^{2+} events that lasted 4 s and longer. The experiments were performed in baseline conditions (i.e. without any blockers) or after exposing the slice to 100 μM of gap junction/hemichannel blocker

carbenoxolone (CBX). Experiments with CBX aimed to test a possible role of astrocyte uncoupling after CR on cytosolic Ca^{2+} dynamics.

CR decreases the duration and size of Ca^{2+} events

Detected Ca^{2+} events were reconstructed for each slice in three-dimensional space: x-y-time (Fig. 1a). Subsequently, individual events were extracted and analysed (Fig. 1b). Event frequency was calculated as the number of events divided by recording time and by the size of the recording field (frequency density). CR tended to increase Ca^{2+} event frequency; however, the difference did not reach statistical significance (Fig. 1c). Application of CBX affected the frequency neither in the control nor CR group. Event duration was calculated as the number of frames during which the event existed multiplied by the interval between frames. CR significantly decreased Ca^{2+} event duration at baseline recordings (Fig. 1d). The difference in Ca^{2+} event duration between the control and CR group remained significant in the presence of CBX. Application of CBX did not significantly affect the duration in either group. This finding rules out that gap junction uncoupling following CR is responsible for the shortening of Ca^{2+} events in astrocytes. Event size was calculated as the area of maximal intensity projection.

Exposure to CR significantly decreased Ca^{2+} event size at baseline recordings (Fig. 1e). Application of CBX did not significantly affect the size of Ca^{2+} events in the control group but partially reversed the decrease in the Ca^{2+} event size following CR. The difference in Ca^{2+} event size between the control and CR group, however, remained significant in the presence of CBX.

CR decreases the expansion and shrinkage rates of Ca^{2+} events

Other properties of Ca^{2+} events are the rates at which they expand and shrink (Fig. 2a). From all Ca^{2+}event we detected some were spreading, while the rest remained local. Neither CR nor CBX affected the proportion of spreading events (Fig. 2b). Then we measured the area occupied by the Ca^{2+} event in each frame and obtained the time course of the Ca^{2+} event area (Fig. 2c). In this time course, we identified the expansion phase and the shrinkage phase, from which expansion and shrinkage rates were calculated. Exposure to CR significantly decreased the expansion rate of Ca^{2+} events (Fig. 2d). Treatment with CBX had no significant effect on the rate in the control group but increased it in the CR group. As a result, expansion rates in control and CR groups became not significantly different in CBX treated slices. Similarly, the Ca^{2+} event shrinkage rate was significantly reduced following CR (Fig. 2e). Treatment with CBX, however, significantly affected shrinkage rate neither in control nor in the CR group. Hence, the difference between shrinkage rate in control and in CR groups remained in CBX treated slices. These results suggest that the reduction of Ca^{2+} event sizes following CR may be explained by reduced expansion and shrinkage rates. Blockade of gap junctions/hemichannel reverses the effect of CR on event size and expansion rate, but not on event duration. Reduced event duration following CR may reflect changes in astrocyte morphology or involvement of other mechanisms.

CR increases the amplitude and accelerates the rise and decay rates of Ca^{2+} signals

Astrocytic Ca^{2+} events can be characterised in multiple dimensions within space and time [8]. In addition to spatiotemporal properties (size and duration) and spatiotemporal dynamics (expansion and shrinkage rates), we characterised the amplitude ($\Delta F/F$) and the waveform (rise and decay rates) of the Ca^{2+} signal (Fig. 3a). Since different pixels within the event have different Ca^{2+} timecourse, we have identified the maximal amplitude, rise and decay rates within the event. CR increased the amplitude of Ca^{2+} signals (Fig. 3b). Treatment with CBX further increased the amplitude of $[Ca^{2+}]_i$ increase in control but not in CR groups. As a result, the difference between groups disappeared. Similar to the amplitude, rise and decay rates of Ca^{2+} signals were increased following CR (Fig. 3c,d). Exposure to CBX increased the rates both in control and CR groups. Hence, the difference between groups, however, remained.

Discussion

In this study, we analysed spatiotemporal profiles of $[Ca^{2+}]_i$ signals in hippocampal astrocytes from animals exposed to CR, which is known to boost adaptive capabilities of various organisms, counteract age-dependent cognitive decline and decrease the risk for neurodegenerative diseases [30-32]. Exposure to CR decreased the size and duration of Ca^{2+} events; these Ca^{2+} events also demonstrated slower expansion and shrinkage rates. In other words, slower expanding Ca^{2+} events occupy the smaller territory as compared to more rapidly expanding events. However, at present, we have not determined a mechanism that is responsible for the reduced size of events. We also observed that the frequency of Ca^{2+} events tends to increase after CR. Although the increase in frequency did not reach significance, it compensated for smaller size of Ca^{2+} events: the mean percentage of each frame covered by Ca^{2+} events was not statistically different between control and CR. This finding suggests that CR made Ca^{2+} events more localised and "concentrated", but it does not affect overall Ca^{2+} activity. What could that mean from the point of astrocytic physiology or brain computation? Recent reports demonstrated the importance of astrocytic microdomains for animal memory consolidation [33]. Since each astrocytic Ca^{2+} microdomain occurs in compartments covering a different number of synapses, the latter can be simultaneously co-modulated [8, 34]. In this scenario, a reduction in the size of the Ca^{2+} event may, conceivably, reduce clusters of co-modulated synapses. At the same time, CR increases the amplitude and accelerates the kinetics of both rise and decay of local $[Ca^{2+}]_i$ transients. Thus, in animals under diet, Ca^{2+} signals become sharper and more localised. Their modulatory action of synapses may be stronger. This can be potentially linked to the precision of information coding in the neuronal network and warrants further analysis.

Spatiotemporal $[Ca^{2+}]_i$ dynamics is a fundamental component for astrocytic intracellular excitability [1, 5]. Local $[Ca^{2+}]_i$ microdomains are critically important for astrocyte physiology being involved in the regulation of ATP production (stimulus-metabolic coupling), gene expression, cell development and death (short and long-term adaptation) or exocytosis (stimulus-secretion couplings), to name a few Ca^{2+}-dependent processes [8, 35]. Generation and shaping of Ca^{2+} signals in a highly complex astrocytic arborisation is

determined by an interplay between plasmalemmal Ca^{2+} entry (mediated by Ca^{2+}-permeable ionotropic receptors, reversed Na^{+}/Ca^{2+} exchanger, store-operated Ca^{2+} channels) intracellular Ca^{2+} release from intracellular Ca^{2+} stores (mainly associated with the opening of $InsP_3/Ca^{2+}$-gated Ca^{2+} release channels of the endoplasmic reticulum), cytoplasmic Ca^{2+} buffering by Ca^{2+} binding proteins and by Ca^{2+} extrusion mediated by plasmalemmal Ca^{2+} pumps and Na^{+}/Ca^{2+} exchanger running in the forward mode [5, 6, 16]. All these molecular pathways operate within astrocytic compartments represented by organelle containing soma and primary processes, known as branches and organelle-free thin distal processes defined as leaflets [1, 8, 9, 36]. Generation of Ca^{2+} signalling in these two compartments is relatively independent with leaflets relying mainly on Ca^{2+} influx, whereas in branches Ca^{2+} release from the internal Ca^{2+} stores plays the leading role [1, 37-39]. These two principal compartments of astrocyte have another distinct morphological feature associated with the surface to volume ratio (SVR), which is high in leaflets and is much smaller in branches and in the soma. In addition, spatiotemporal properties of astrocytic $[Ca^{2+}]_i$ dynamics may be influenced by gap junctional syncytia connectivity that provides diffusion of second messengers which can create propagating Ca^{2+} waves [18].

All these arguments demonstrate that changes in astrocyte morphology and particularly changes in the morphology of their processes, both primary and distal, may substantially affect spatiotemporal $[Ca^{2+}]_i$ landscapes. Previous studies have demonstrated such a morphofunctional relation [14, 27]. It appears that spontaneous Ca^{2+} events appear more frequently in distal processes with higher SVR compare to the branches with lower SVR. Astrocytic processes are morphologically dynamic structures, which can extend or retract both in short and long-term temporal domains, thus affecting and regulating neurotransmitter dynamics and synaptic plasticity [20, 21]. The long-term brain adaptation associated with, for example, dieting [26], physical exercise [24, 40] and ageing [22, 41] all result in substantial morphological remodelling of astrocytes. Ageing and caloric restriction, in particular, mainly affect distal astrocytic leaflets [23, 26], which arguably form the majority of perisynaptic astrocytic contacts. These latter are fundamental to synaptic function through regulation of synaptogenesis, and providing for synaptic maintenance, synaptic isolation and synaptic extinction [19, 42].

What are molecular and cellular mechanisms responsible for such remodelling of astrocytic Ca^{2+} activity following CR? There could be numerous possibilities at molecular, cellular and network levels. Previous studies have demonstrated a relationship between astrocyte morphology and Ca^{2+} dynamics [27, 34]. It appears that spontaneous Ca^{2+} events are more frequent in distal processes with a higher surface-to-volume ratio (SVR) compared to the branches with lower SVR. Indeed, CR triggers astrocyte growth which can thus affect Ca^{2+} activity [26]. Gap-junction coupling has been suggested as a Ca^{2+} signal propagation pathway in astrocytic syncytium [5, 43]. Exposure to the CR reduces astrocytic coupling through gap junctions [26], which may explain the reduced size of Ca^{2+} events. Gap junction blocker, CBX did not impact on $[Ca^{2+}]_i$ dynamics in the control mice; in the CR group, CBX partially rescued the decrease in the size of Ca^{2+} event in CR animals. This finding was unexpected since we assumed that CBX should mimic astrocyte uncoupling in the control group and hence have more effect than in the

CR group. However, CBX not only prevents the coupling of astrocytes through gap junctions but also blocks hemichannels. Assuming astrocyte uncoupling following CR exposes more hemichannels previously used in gap junctions may explain why CBX (by blocking hemichannels) has a more substantial effect in the CR group.

In summary, the results show remodelling of Ca^{2+} activity in hippocampal astrocytes following CR. Ca^{2+} events became shorter and smaller in size. The smaller size may be explained by slower expansion and shrinkage rates of the events. On the other hand, CR increased the amplitude, rise and decay rates of Ca^{2+} signal. These changes were partially reversed by the action of CBX, pointing to the role of gap junctions or hemichannels. Unexpectedly, CBX had a more profound effect on the CR group, where gap junction coupling between astrocytes is reduced [26]. This suggests that uncoupling may lead to an increased number of hemichannels that are responsible for Ca^{2+} events confined in space and time with higher Ca^{2+} content. How these changes in Ca^{2+} spatiotemporal landscape may translate into astrocytic physiology remains a matter for future studies.

Acknowledgements

The work was supported by the Russian Science Foundation grant 20-14-00241 to AS.

References

[1] A. Verkhratsky, A. Semyanov, R. Zorec, Physiology of astroglial excitability, Function, 1 (2020) zqaa016.
[2] A.C. Charles, J.E. Merrill, E.R. Dirksen, M.J. Sanderson, Intercellular signaling in glial cells: calcium waves and oscillations in response to mechanical stimulation and glutamate, Neuron, 6 (1991) 983-992.
[3] A.H. Cornell-Bell, S.M. Finkbeiner, M.S. Cooper, S.J. Smith, Glutamate induces calcium waves in cultured astrocytes: long-range glial signaling, Science, 247 (1990) 470-473.
[4] M.O. Enkvist, I. Holopainen, K.E. Akerman, Glutamate receptor-linked changes in membrane potential and intracellular Ca^{2+} in primary rat astrocytes, Glia, 2 (1989) 397-402.
[5] A. Semyanov, Spatiotemporal pattern of calcium activity in astrocytic network, Cell Calcium, 78 (2019) 15-25.
[6] A. Verkhratsky, J.J. Rodriguez, V. Parpura, Calcium signalling in astroglia, Mol Cell Endocrinol, 353 (2012) 45-56.
[7] X. Yu, J. Nagai, B.S. Khakh, Improved tools to study astrocytes, Nat Rev Neurosci, 21 (2020) 121-138.
[8] A. Semyanov, C. Henneberger, A. Agarwal, Making sense of astrocytic calcium signals - from acquisition to interpretation, Nat Rev Neurosci, 21 (2020) 551-564.
[9] B.S. Khakh, M.V. Sofroniew, Diversity of astrocyte functions and phenotypes in neural circuits, Nat Neurosci, 18 (2015) 942-952.
[10] A. Agarwal, P.H. Wu, E.G. Hughes, M. Fukaya, M.A. Tischfield, A.J. Langseth, D. Wirtz, D.E. Bergles, Transient Opening of the Mitochondrial Permeability Transition Pore Induces Microdomain Calcium Transients in Astrocyte Processes, Neuron, 93 (2017) 587-605 e587.
[11] J. Kwon, H. An, M. Sa, J. Won, J.I. Shin, C.J. Lee, Orai1 and Orai3 in Combination with Stim1 Mediate the Majority of Store-operated Calcium Entry in Astrocytes, Exp Neurobiol, 26 (2017) 42-54.
[12] A.B. Toth, K. Hori, M.M. Novakovic, N.G. Bernstein, L. Lambot, M. Prakriya, CRAC channels regulate astrocyte Ca^{2+} signaling and gliotransmitter release to modulate hippocampal GABAergic transmission, Sci Signal, 12 (2019).
[13] A. Verkhratsky, V. Parpura, Store-operated calcium entry in neuroglia, Neurosci Bull, 30 (2014) 125-133.
[14] R.L. Rungta, L.P. Bernier, L. Dissing-Olesen, C.J. Groten, J.M. LeDue, R. Ko, S. Drissler, B.A. MacVicar, Ca^{2+} transients in astrocyte fine processes occur via Ca^{2+} influx in the adult mouse hippocampus, Glia, 64 (2016) 2093-2103.
[15] E. Shigetomi, O. Jackson-Weaver, R.T. Huckstepp, T.J. O'Dell, B.S. Khakh, TRPA1 channels are regulators of astrocyte basal calcium levels and long-term potentiation via constitutive D-serine release, J Neurosci, 33 (2013) 10143-10153.
[16] C.R. Rose, D. Ziemens, A. Verkhratsky, On the special role of NCX in astrocytes: Translating Na^{+}-transients into intracellular Ca^{2+} signals, Cell Calcium, 86 (2020) 102154.

[17] O. Palygin, U. Lalo, A. Verkhratsky, Y. Pankratov, Ionotropic NMDA and $P2X_{1/5}$ receptors mediate synaptically induced Ca^{2+} signalling in cortical astrocytes, Cell Calcium, 48 (2010) 225-231.
[18] C. Giaume, C.C. Naus, J.C. Saez, L. Leybaert, Glial Connexins and Pannexins in the Healthy and Diseased Brain, Physiol Rev, 101 (2021) 93-145.
[19] M. Augusto-Oliveira, G.P. Arrifano, P.Y. Takeda, A. Lopes-Araujo, L. Santos-Sacramento, D.C. Anthony, A. Verkhratsky, M.E. Crespo-Lopez, Astroglia-specific contributions to the regulation of synapses, cognition and behaviour, Neurosci Biobehav Rev, 118 (2020) 331-357.
[20] C. Henneberger, L. Bard, A. Panatier, J.P. Reynolds, O. Kopach, N.I. Medvedev, D. Minge, M.K. Herde, S. Anders, I. Kraev, J.P. Heller, S. Rama, K. Zheng, T.P. Jensen, I. Sanchez-Romero, C.J. Jackson, H. Janovjak, O.P. Ottersen, E.A. Nagelhus, S.H.R. Oliet, M.G. Stewart, U.V. Nagerl, D.A. Rusakov, LTP Induction Boosts Glutamate Spillover by Driving Withdrawal of Perisynaptic Astroglia, Neuron, (2020).
[21] D.T. Theodosis, D.A. Poulain, S.H. Oliet, Activity-dependent structural and functional plasticity of astrocyte-neuron interactions, Physiol Rev, 88 (2008) 983-1008.
[22] A. Verkhratsky, M. Augusto-Oliveira, A. Pivoriunas, A. Popov, A. Brazhe, A. Semyanov, Astroglial asthenia and loss of function, rather than reactivity, contribute to the ageing of the brain, Pflugers Arch, (2020).
[23] A. Popov, A. Brazhe, P. Denisov, O. Sutyagina, L. Li, N. Lazareva, A. Verkhratsky, A. Semyanov, Astrocyte dystrophy in ageing brain parallels impaired synaptic plasticity, Aging Cell, 20 (2021) e13334.
[24] J.J. Rodriguez, S. Terzieva, M. Olabarria, R.G. Lanza, A. Verkhratsky, Enriched environment and physical activity reverse astrogliodegeneration in the hippocampus of AD transgenic mice, Cell Death Dis, 4 (2013) e678.
[25] M. Augusto-Oliveira, A. Verkhratsky, Mens sana in corpore sano: lifestyle changes modify astrocytes to contain Alzheimer's disease, Neural Regen Res, 16 (2021) 1548-1549.
[26] A. Popov, P. Denisov, M. Bychkov, A. Brazhe, E. Lyukmanova, Z. Shenkarev, N. Lazareva, A. Verkhratsky, A. Semyanov, Caloric restriction triggers morphofunctional remodeling of astrocytes and enhances synaptic plasticity in the mouse hippocampus, Cell Death Dis, 11 (2020) 208.
[27] Y.W. Wu, S. Gordleeva, X. Tang, P.Y. Shih, Y. Dembitskaya, A. Semyanov, Morphological profile determines the frequency of spontaneous calcium events in astrocytic processes, Glia, 67 (2019) 246-262.
[28] M. Makitalo, A. Foi, Optimal inversion of the Anscombe transformation in low-count Poisson image denoising, IEEE Trans Image Process, 20 (2011) 99-109.
[29] M. Tepper, G. Sapiro, L1 Splines for Robust, Simple, and Fast Smoothing of Grid Data, arXiv, 1208.2292 (2012).
[30] M.P. Mattson, Energy intake and exercise as determinants of brain health and vulnerability to injury and disease, Cell Metab, 16 (2012) 706-722.
[31] L. Fontana, L. Partridge, V.D. Longo, Extending healthy life span--from yeast to humans, Science, 328 (2010) 321-326.
[32] M. Maalouf, J.M. Rho, M.P. Mattson, The neuroprotective properties of calorie restriction, the ketogenic diet, and ketone bodies, Brain Res Rev, 59 (2009) 293-315.

[33] B. Vignoli, G. Sansevero, M. Sasi, R. Rimondini-Giorgini, R. Blum, S. Santi, N. Berardi, B. Lu, M. Canossa, Astrocytic Microdomains Confine A “molecular Memory” Enabling Long-Term Information Storage for Memory Consolidation, ReserachSquare, Preprint (2021).
[34] Y.W. Wu, X. Tang, M. Arizono, H. Bannai, P.Y. Shih, Y. Dembitskaya, V. Kazantsev, M. Tanaka, S. Itohara, K. Mikoshiba, A. Semyanov, Spatiotemporal calcium dynamics in single astrocytes and its modulation by neuronal activity, Cell Calcium, 55 (2014) 119-129.
[35] A. Verkhratsky, M. Nedergaard, Physiology of Astroglia, Physiol Rev, 98 (2018) 239-389.
[36] A.A. El Alaoui, M. Jackson, M. Fabri, L. de Vivo, M. Bellesi, Characterization of Subcellular Organelles in Cortical Perisynaptic Astrocytes, Front. Cell. Neurosci, 14 (2021) a573944.
[37] K. Kanemaru, J. Kubota, H. Sekiya, K. Hirose, Y. Okubo, M. Iino, Calcium-dependent N-cadherin up-regulation mediates reactive astrogliosis and neuroprotection after brain injury, Proc Natl Acad Sci U S A, 110 (2013) 11612-11617.
[38] J. Petravicz, K.M. Boyt, K.D. McCarthy, Astrocyte IP_3R2-dependent Ca^{2+} signaling is not a major modulator of neuronal pathways governing behavior, Front Behav Neurosci, 8 (2014) 384.
[39] R. Srinivasan, B.S. Huang, S. Venugopal, A.D. Johnston, H. Chai, H. Zeng, P. Golshani, B.S. Khakh, Ca^{2+} signaling in astrocytes from $Ip3r2^{-/-}$ mice in brain slices and during startle responses *in vivo*, Nat Neurosci, 18 (2015) 708-717.
[40] D.G. Diniz, M.A. de Oliveira, C.M. de Lima, C.A. Foro, M.C. Sosthenes, J. Bento-Torres, P.F. da Costa Vasconcelos, D.C. Anthony, C.W. Diniz, Age, environment, object recognition and morphological diversity of GFAP-immunolabeled astrocytes, Behav Brain Funct, 12 (2016) 28.
[41] J.J. Rodriguez, C.Y. Yeh, S. Terzieva, M. Olabarria, M. Kulijewicz-Nawrot, A. Verkhratsky, Complex and region-specific changes in astroglial markers in the aging brain, Neurobiol Aging, 35 (2014) 15-23.
[42] A. Verkhratsky, M. Nedergaard, Astroglial cradle in the life of the synapse, Philos Trans R Soc Lond B Biol Sci, 369 (2014) 20130595.
[43] Y. Fujii, S. Maekawa, M. Morita, Astrocyte calcium waves propagate proximally by gap junction and distally by extracellular diffusion of ATP released from volume-regulated anion channels, Sci Rep, 7 (2017) 13115.

Figure legends

Figure 1. CR reduces both size and duration of astrocytic Ca^{2+} events.

a. Recording astrocytic Ca^{2+} activity in hippocampal CA1 *stratum radiatum*. All Ca^{2+} events were detected and presented in the x-y-time volume, where the bottom illustrates the fluorescent image and the vertical axis of the time. Each Ca^{2+} event occurs in time and space.

b. Individual Ca^{2+} event zoomed from the boxed area at the panel a. The duration of the event is calculated as the number of frames when the event was detected multiplied by the interframe interval. The event duration calculated as the area of event maximal intensity projection (MIP) along the time axis.

c. Frequency of Ca^{2+} events normalised to the imaging area (frequency density) at baseline conditions (N = 6 in control, green, and N = 5 in CR, grey) and in the presence of carbenoxolone, CBX (N = 7 in control and N = 5 in CR). CR did not significantly affect the frequency (p=0.11); CBX did not significantly affect the frequency (p=0.77); there was no significant interaction between the effects of CR and CBX (p=0.58). Two-way repeated-measures ANOVA.

d. Ca^{2+} event duration at baseline conditions (N = 6, n = 239 in control, green, and N = 5, n = 327 in CR, grey; p = 0.002 between control and CR) and in the presence of carbenoxolone, CBX (N = 7, n = 201 in control and N = 5, n = 354 in CR; p = 0.025 between control and CR). CBX did not have statistically significant effect on either control (p = 0.84) or CR group (p = 0.25). Mann-Whitney test.

e. Ca^{2+} event size at baseline conditions (N = 6, n = 239 in control, green, and N = 5, n = 327 in CR, grey; p < 0.001 between control and CR) and in the presence of carbenoxolone, CBX (N = 7, n = 201 in control and N = 5, n = 354 in CR; p < 0.001 between control and CR). CBX did not have statistically significant effect on control (p = 0.44) but on CR group (p < 0.001). Mann-Whitney test.

The data are presented as quartiles (box) ± 10th and 90th percentiles (whiskers), except for panel c, where data are presented as the mean ± SEM. N – number of slices (animals), n – number of recorded Ca^{2+} events; ns – p > 0.05, * - p < 0.05, ** - p < 0.01, *** - p < 0.001.

Figure 2. CR reduces the expansion and shrinkage rates of astrocytic Ca^{2+} events.

a. Time-lapse imaging (1 frame/s) of an expanding Ca^{2+} event. The event was binarised to illustrate changes in its area.

b. Percentage of expanding Ca^{2+} events at baseline conditions (N = 6 in control, green, and N = 5 in CR, grey) and in the presence of carbenoxolone, CBX (N = 7 in control and N = 5 in CR). CBX did not have a statistically significant effect on either control or CR group. Two-sample *t*-test.

c. The timecourse of the change in the area of Ca^{2+} event shown at the panel a. Red – expansion phase, blue – shrinkage phase.

d. Ca^{2+} event expansion rate at baseline conditions (N = 6, n = 184 in control, green, and N = 5, n = 214 in CR, grey; $p < 0.001$ between control and CR) and in the presence of carbenoxolone, CBX (N = 7, n = 142 in control and N = 5, n = 227 in CR; $p = 0.06$ between control and CR). CBX did not have statistically significant effect on control ($p = 0.36$) but on CR group ($p = 0.024$). Mann-Whitney test. Data presented for expanding events only.

d. Ca^{2+} event shrinkage rate at baseline conditions (N = 6, n = 184 in control, green, and N = 5, n = 214 in CR, grey; $p < 0.001$ between control and CR) and in the presence of carbenoxolone, CBX (N = 7, n = 142 in control and N = 5, n = 227 in CR; $p = 0.002$ between control and CR). CBX did not have statistically significant effect on control ($p = 0.06$) or CR group ($p = 0.59$). Mann-Whitney test. Data presented for expanding events only.

The data are presented as quartiles (box) ± 10th and 90th percentiles (whiskers). N – number of slices (animals), n – number of recorded Ca^{2+} events; ns – $p > 0.05$, * - $p < 0.05$, ** - $p < 0.01$, *** - $p < 0.001$.

Figure 3. CR increases the amplitude of the Ca^{2+} signal and Ca^{2+} rise and decay rates.

a. Time-lapse imaging (1 frame/s) of an expanding Ca^{2+} event. *Top row,* the event was presented in pseudocolor to illustrate the amplitude (ΔF/F) of the fluorescent signal in each pixel forming the event. The background is an original fluorescent signal showing astrocyte morphology. MIP – maximal intensity projection. *Bottom row,* each pixel of the event presented in red when the fluorescent signal increases and in blue when it decreases. The colour intensity illustrates the rate of the rise or decay of the signal.

b. Maximal Ca^{2+} signal amplitude within the event at baseline conditions (N = 6, n = 239 in control, green, and N = 5, n = 327 in CR, grey; $p < 0.001$ between control and CR) and in the presence of carbenoxolone, CBX (N = 7, n = 201 in control and N = 5, n = 354 in CR; $p = 0.26$ between control and CR). CBX had statistically significant effect on control ($p < 0.001$) but not on CR group ($p = 0.06$). Mann-Whitney test.

c. Maximal rise rate of Ca^{2+} signal within the event at baseline conditions (N = 6, n = 239 in control, green, and N = 5, n = 327 in CR, grey; $p < 0.001$ between control and CR) and in the presence of carbenoxolone, CBX (N = 7, n = 201 in control and N = 5, n = 354 in CR; $p < 0.001$ between control and CR). CBX had statistically significant effect on both control ($p < 0.001$) and on CR group ($p < 0.001$). Mann-Whitney test.

d. Maximal decay rate of Ca^{2+} signal within the event at baseline conditions (N = 6, n = 239 in control, green, and N = 5, n = 327 in CR, grey; $p < 0.001$ between control and CR) and in the presence of carbenoxolone, CBX (N = 7, n = 201 in control and N = 5, n = 354 in CR; $p < 0.001$ between control and CR). CBX had statistically significant effect on both control ($p < 0.001$) and on CR group ($p < 0.001$). Mann-Whitney test.

The data are presented as quartiles (box) ± 10th and 90th percentiles (whiskers). N – number of slices (animals), n – number of recorded Ca^{2+} events; ns – $p > 0.05$, *** - $p < 0.001$.

Figure 1

Click here to access/download;Figure;Figure-01.tif

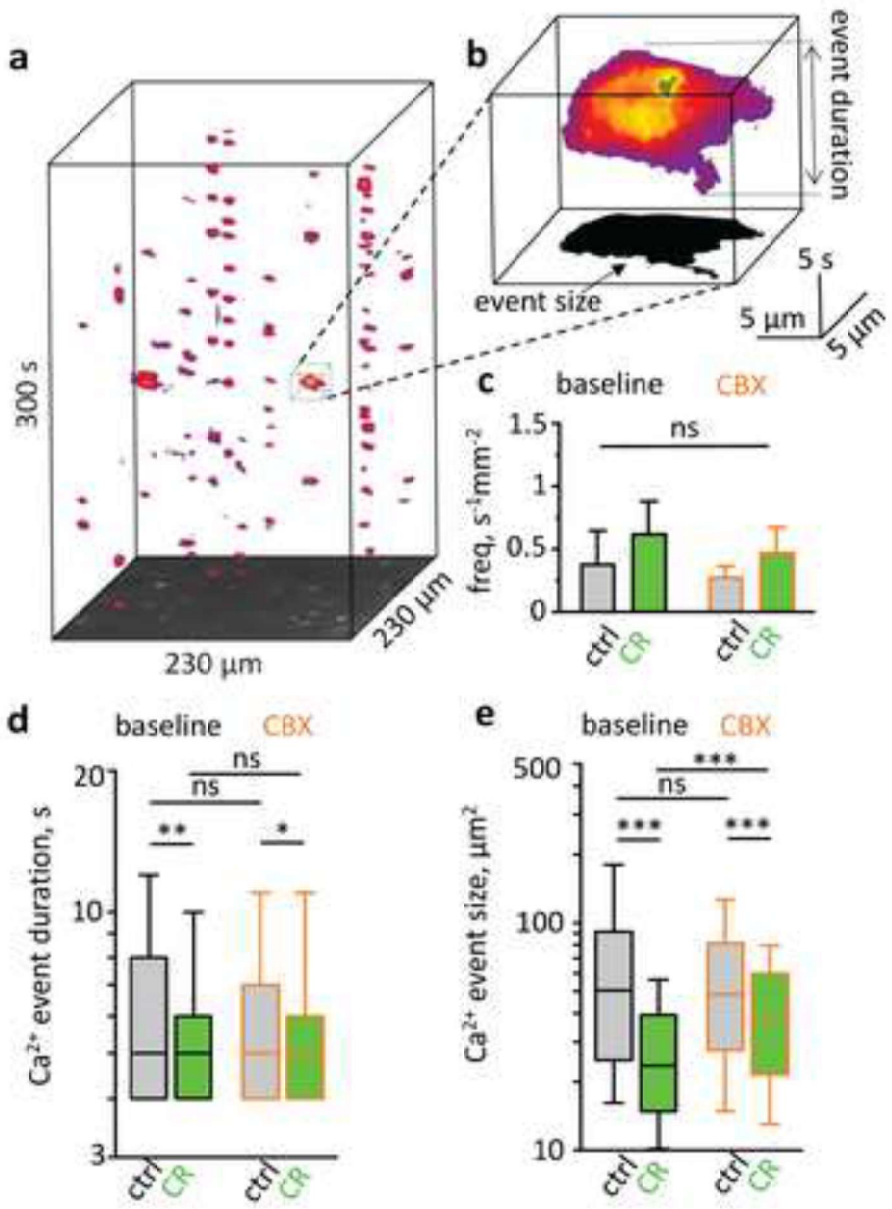

Figure 2

Click here to access/download;Figure;Figure-02.tif

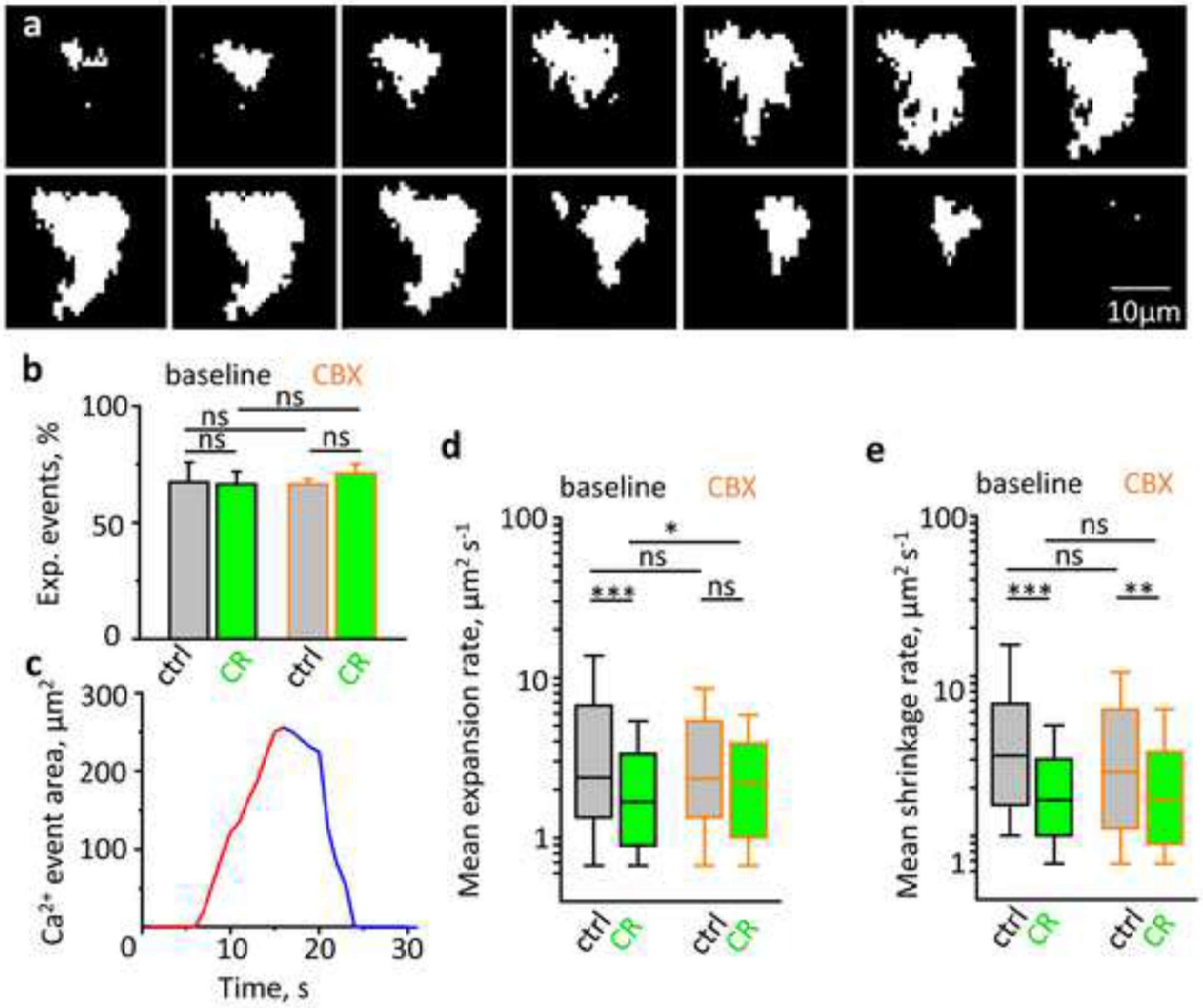

Figure 3

Click here to access/download;Figure;Figure-03.tif